

NASA CONTRACTOR
REPORT

NASA CR-178967

COMPUTATION OF TURBULENT BOUNDARY LAYER FLOWS
WITH AN ALGEBRAIC STRESS TURBULENCE MODEL

By Sang-Wook Kim and Yen-Sen Chen
Universities Space Research Association
Science and Engineering Directorate
Systems Dynamics Laboratory

Final Report

November 1986

Prepared for
NASA-Marshall Space Flight Center
Marshall Space Flight Center, Alabama 35812

(NASA-CR-178967) COMPUTATION OF TURBULENT
BOUNDARY LAYER FLOWS WITH AN ALGEBRAIC
STRESS TURBULENCE MODEL (Universities Space
Research Association) 25 p CSCL 20D

N87-16982

Unclas
G3/34 43854

1. REPORT NO. NASA CR-178967	2. GOVERNMENT ACCESSION NO.	3. RECIPIENT'S CATALOG NO.	
4. TITLE AND SUBTITLE Computation of Turbulent Boundary Layer Flows With an Algebraic Stress Turbulence Model		5. REPORT DATE November 1986	
		6. PERFORMING ORGANIZATION CODE	
7. AUTHOR(S) Sang-Wook Kim* and Yen-Sen Chen*		8. PERFORMING ORGANIZATION REPORT #	
9. PERFORMING ORGANIZATION NAME AND ADDRESS George C. Marshall Space Flight Center Marshall Space Flight Center, Alabama 35812		10. WORK UNIT NO.	
		11. CONTRACT OR GRANT NO. NAS8-35918	
12. SPONSORING AGENCY NAME AND ADDRESS National Aeronautics and Space Administration Washington, D.C. 20546		13. TYPE OF REPORT & PERIOD COVERED Contractor Report	
		14. SPONSORING AGENCY CODE	
15. SUPPLEMENTARY NOTES Prepared by Fluid Dynamics Branch, Systems Dynamics Laboratory, Science and Engineering Directorate. * Universities Space Research Association.			
16. ABSTRACT An algebraic stress turbulence model is presented. The model can be characterized by the following three aspects: (1) the eddy viscosity expression is derived from the Reynolds stress turbulence model; (2) the turbulent kinetic energy dissipation rate equation is improved by including a production range time scale; and (3) the diffusion coefficients for turbulence equations are adjusted so that the kinetic energy profile extends further into the free stream region which can be found in most experimental data. The turbulent flow equations were solved using a finite element method. Example problems considered include: a fully developed channel flow, a fully developed pipe flow, a flat plate boundary layer flow, a plane jet exhausting into a moving stream, a circular jet exhausting into a moving stream, and a wall jet flow. Computational results compare favorably with experimental data for most of the example problems considered. Significantly improved computational results were obtained for the plane jet flow, the circular jet flow, and the wall jet flow; whereas the remainder of the computational results are comparable to those obtained by finite difference methods using the standard $k-\epsilon$ turbulence model. The turbulence model seems to be promising with further improvement of the expression for the eddy viscosity coefficient.			
17. KEY WORDS Turbulent Boundary Layer Flows Algebraic Stress Turbulence Model Finite Element Method Wall Jet Flow		18. DISTRIBUTION STATEMENT Unclassified-Unlimited	
19. SECURITY CLASSIF. (of this report) Unclassified	20. SECURITY CLASSIF. (of this page) Unclassified	21. NO. OF PAGES 24	22. PRICE NTIS

TABLE OF CONTENTS

	Page
INTRODUCTION	1
TURBULENCE MODEL.....	2
Eddy Viscosity Equation	2
Dissipation Rate Equation	2
Diffusion Coefficients for Turbulence Quantities.....	4
TURBULENT FLOW EQUATIONS.....	5
FINITE ELEMENT COMPUTATIONAL PROCEDURE.....	5
COMPUTATIONAL RESULTS	6
CONCLUSIONS	18
REFERENCES	19

PRECEDING PAGE BLANK NOT FILMED

LIST OF ILLUSTRATIONS

Figure	Title	Page
1.	C_μ function	3
2.	Fully developed channel flow	7
3.	Fully developed pipe flow.....	8
4.	Wall shearing stress for the flat plate flow.....	9
5.	Flat plate flow with zero pressure gradient	10
6.	A plane jet exhausting into a moving stream	11
7.	A plane jet exhausting into a moving stream	12
8.	A circular jet exhausting into a moving stream.....	13
9.	A circular jet exhausting into a moving stream.....	15
10.	Configuration of a wall-jet flow	16
11.	A wall-jet flow	16
12.	A wall-jet flow	17

CONTRACTOR REPORT

COMPUTATION OF TURBULENT BOUNDARY LAYER FLOWS WITH AN ALGEBRAIC STRESS TURBULENCE MODEL

INTRODUCTION

During the last decades, significant progress has been made in mathematically modeling the turbulent flows. Memorable events in the effort, among many others, would be the two Stanford Conferences on turbulent flows [1,2].

Development of turbulence models, and accordingly computation of turbulent flows too, were made, entirely to certain extents, using one or another form of the finite difference computational method. Only very recently, a few publications on finite element computation of turbulent flows begin to appear.

A list of publications on finite element computation of turbulent flows can be found in Reference 3. To summarize, finite element computation of turbulent flows resulted in, more or less, dissatisfaction in most of the cases. The turbulent kinetic energy or dissipation rate becomes negative during iterative solution procedure so that a dedicated computational procedure to overcome this difficulty has also been proposed [4]. The hardly obtained computational results were less satisfactory than that of the finite difference computation of the same turbulent flow using the same turbulence model in some cases [4]. Considering the success of the finite element method in other areas of engineering computations, such as the structural mechanics, laminar flow problems, and chemical process modelings to mention a few, it is quite unusual that the finite element method can hardly be used for computation of turbulent flows especially when $k-\epsilon$ type turbulence models are used. But it should be mentioned here that there already exist commercial finite element flow analysis codes using the mixing length turbulence models [5].

A mathematically rigorous finite element turbulent boundary layer flow analysis code has been constructed, which is based on the finite element laminar boundary layer flow analysis code, to assess and/or validate turbulence models to be used for general finite element computation of turbulent flows [3].

It was found that the flow field variables (velocity, turbulent kinetic energy, and dissipation rate) can hardly make smooth transition from the near wall high turbulence region to the free stream low turbulence region in most of the finite element computations. This difficulty was able to be removed by employing a type of algebraic stress turbulence model. The remaining propositions included in the present turbulence model contribute to improving the computational results for turbulent boundary layer flows. Use of the present turbulence model in finite difference computation of turbulent boundary layer flows, as well as elliptic flows, improved the computational results compared with those obtained by using the standard $k-\epsilon$ turbulence models [7].

It would be worthwhile to mention that most of the $k-\epsilon$ turbulence models were able to run smoothly in the present finite element turbulent boundary layer flow code (BLFLOW) [3] simply by including the algebraic stress form of the eddy viscosity into those turbulence models. In this regard, the observed differences between the two numerical methods are also discussed in this report.

TURBULENCE MODEL

Eddy Viscosity Equation

The eddy viscosity expression can be obtained by contracting the Reynolds stress turbulence model [8] using an algebraic Reynolds stress transport assumption [9]. In most of the algebraic stress turbulence models, the eddy viscosity is given as [9,10]:

$$\nu_t = c_\mu k^2/\varepsilon \quad (1)$$

$$c_\mu = \frac{2}{3} \frac{(1-c_{v2}) (c_{v1} - 1 + c_{v2} P/\varepsilon)}{(c_{v1} - 1 + P/\varepsilon)^2} \quad (2)$$

where ν_t is the turbulent eddy viscosity; k is the turbulent kinetic energy; ε is the dissipation rate; P , $P = \nu_t (\partial u / \partial y)^2$, is the production rate; u is the time averaged flow direction velocity; y is the transverse coordinate; $c_{v1} = 3.7 + 0.7 \tanh(P/\varepsilon)$; and $c_{v2} = 0.32$.

The functional form of c_{v1} was used to bring down c_μ to 0.09 for equilibrium state (production rate is equal to the dissipation rate of turbulent kinetic energy). The c_μ curve is shown in Figure 1 together with that of Launder [10]. A different c_μ curve can also be found in Rodi [9]. Experimentally deduced c_μ curves [9] are also shown in Figure 1. It can be seen that the values of c_μ at the center region of jets are close to those at equilibrium state for both jets, respectively. The present c_μ function cannot model this phenomenon. The authors are not aware of any turbulence model which can achieve this phenomenon. This defect deteriorates part of the computational results, which is discussed in the following section. Nevertheless, it was found that the c_μ function was definitely required for the present finite element computation of turbulent boundary layer flows to ensure smooth transition of flow field variables (u , k , ε) from the near wall high turbulence region to the free stream low turbulence region. For multi-dimensional elliptic flows, the potential core region constitutes the low turbulence region, and the c_μ function is required for the same reason as before.

It can be seen in Reference 7 that the c_μ function is not required for the finite difference computation of turbulent flows, and that the same turbulence model with constant $c_\mu (=0.09)$ performed much better than the present case.

Dissipation Rate Equation

It has long been recognized that the standard dissipation rate equation is lack of variable energy transfer capability which will transfer more turbulent kinetic energy

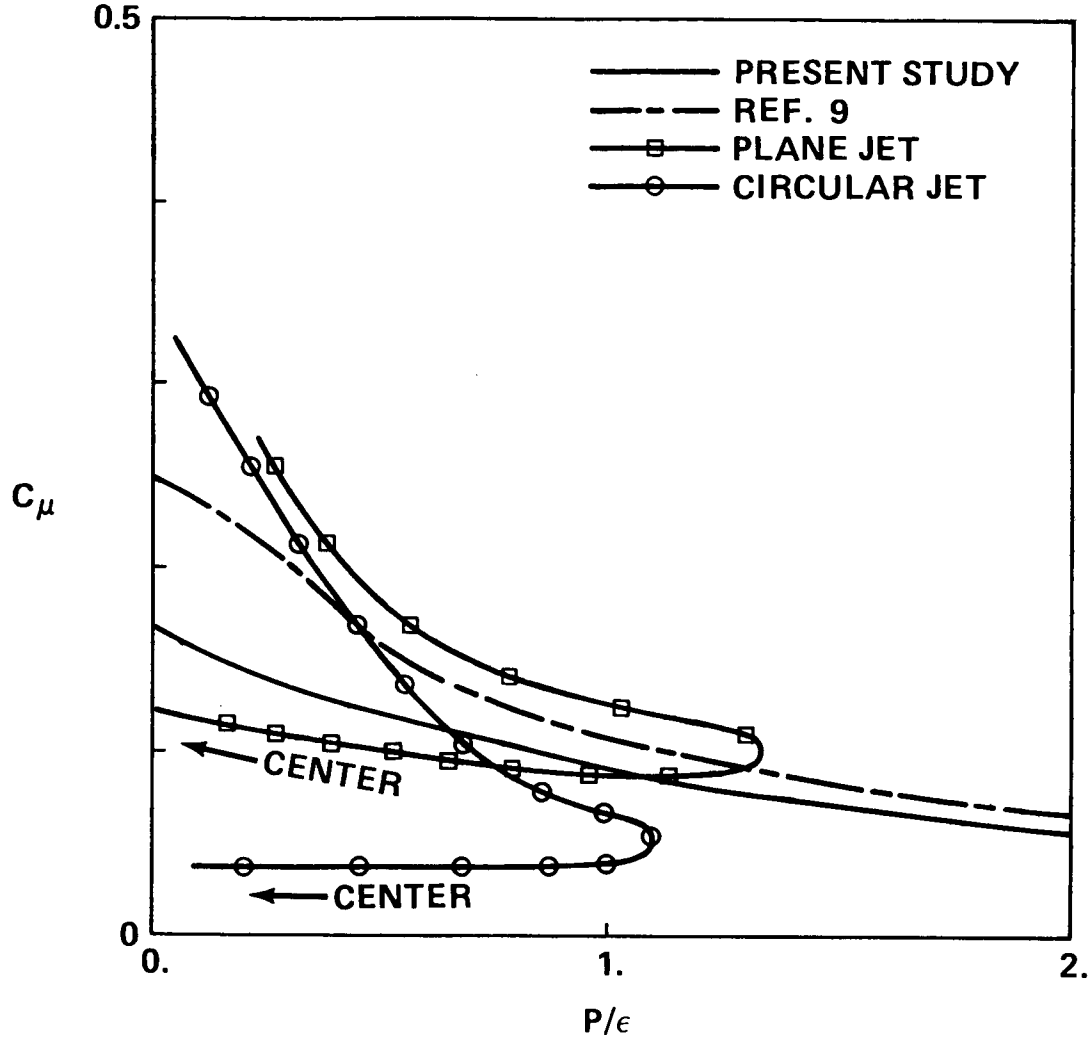


Figure 1. C_μ function.

into dissipation range when production is high. The same line of efforts can be found in Pope [11], Hanjalic and Launder [12], and in Hanjalic et al., [13] among many others.

In the present study, it is proposed to let part of the dissipation rate (ϵ) evolve according to a time-scale related to the production itself. The proposed dissipation rate equation is given as:

$$\frac{D\epsilon}{Dt} = \frac{\epsilon}{k} (c_1' P - c_2' \epsilon) + \frac{P}{k} (c_3' P - c_4' \epsilon) + \frac{1}{y^r} \frac{\partial}{\partial y} \left\{ y^r \left(\nu + \frac{\nu_t}{\sigma_\epsilon} \right) \frac{\partial \epsilon}{\partial y} \right\} \quad (3)$$

where D/Dt represents material derivative; ν is the kinematic viscosity, r is an integer constant such that $r = 0$ for two-dimensional flows and $r = 1$ for axisymmetric flows; and σ_ϵ is a constant. In equation (3), k/ϵ can be considered to be a time scale

related to the dissipation rate; and k/P , to the production rate. After simplification, equation (3) becomes:

$$\frac{D\varepsilon}{Dt} = c_1 \frac{P\varepsilon}{k} - c_2 \frac{\varepsilon^2}{k} + c_3 \frac{P^2}{k} + \frac{1}{y^r} \frac{\partial}{\partial y} \left\{ y^r \left(\nu + \frac{\nu_t}{\sigma_\varepsilon} \right) \frac{\partial \varepsilon}{\partial y} \right\} \quad (4)$$

As usual, (c_1+c_3) may be determined based on the generation rate of dissipation rate as given in Harris et al. [14] and c_2 may be determined according to the decay of grid turbulence experiment of Harlow and Nakayama [15]. The constants used in the present study are: $c_1 = 1.15$, $c_2 = 1.90$, and $c_3 = 0.25$.

Diffusion Coefficients for Turbulence Quantities

Transport equation for turbulent kinetic energy is given as:

$$\frac{Dk}{Dt} = P - \varepsilon + \frac{1}{y^r} \frac{\partial}{\partial y} \left\{ y^r \left(\nu + \frac{\nu_t}{\sigma_k} \right) \frac{\partial k}{\partial y} \right\} \quad (5)$$

Many of the experimental data, such as the flat plate boundary layer flow due to Klebanoff [16] and turbulent jets exhausting into moving streams considered herein as example problems among many others, shows that the turbulent kinetic energy and its gradient are persistently big even after the velocity gradient has vanished near and in the free stream region. It is conjectured that the turbulent kinetic energy has been diffused outward from the high turbulence region due to the following reasons. Firstly, the velocity gradient has vanished and there is no production of turbulent kinetic energy in the region. Secondly, the boundary layer flows are spreading in the downstream direction, hence the turbulent kinetic energy could not have been convected from the upstream region. Thirdly, the decay rate of turbulence, as can be found in the grid turbulence, is so small that the same level of turbulent kinetic energy should exist throughout the free stream region if it has been convected from the high turbulence region. Consequently, the diffusivity of turbulent kinetic energy needs to be bigger than that of the momentum equation, and hence the diffusion coefficient, σ_k , for turbulent kinetic energy was set to be smaller than unit to achieve the observed diffusion process of the turbulent kinetic energy. The proposed values for the model constants are $\sigma_k = 0.75$ and $\sigma_\varepsilon = 1.05$. The value of σ_ε definitely needs to be bigger than σ_k for realizability requirement, i.e., the dissipation rate should decay faster than the turbulent kinetic energy as the free stream region is approached. It was found that $\sigma_k = 1.0$ and $\sigma_\varepsilon = 1.3$, which are most frequently used values in finite difference computations, were acceptable for the present finite element computation even though the diffusion process of turbulent kinetic energy near the free stream region was not so desirable.

TURBULENT FLOW EQUATIONS

For the sake of clarity and completeness, the standard turbulent boundary layer equations are given below.

$$\frac{\partial u}{\partial x} + \frac{1}{y^r} \frac{\partial}{\partial y} (y^r v) = 0 \quad (6)$$

$$u \frac{\partial u}{\partial x} + v \frac{\partial u}{\partial y} - \frac{1}{y^r} \frac{\partial}{\partial y} \left\{ y^r (v + v_t) \frac{\partial u}{\partial y} \right\} = - \frac{dP}{dx} \quad (7)$$

where u and v are time averaged velocities in flow direction and in transverse direction, respectively, and the rest of the notations are the same as before.

FINITE ELEMENT COMPUTATIONAL PROCEDURE

Details of the present finite element computational procedure for turbulent boundary layer flows can be found in References 3 and 6. The coarse grid accuracy reported in Reference 6 was found to hold for the present turbulent boundary layer flow computations too [6]. Only the specific aspects of the present method and the fundamental differences between the finite element [3] and the finite difference method [7] as observed by the authors are described below.

The transverse computational domain was extended outward several times of the boundary layer thicknesses at the initial line of the flow direction computational domain, and orthogonal grids were used everywhere in the flow domain in order to avoid even the slightest source of numerical uncertainty that can be caused by non-orthogonal grid transformation. This scheme is found to be especially helpful in assessing turbulence models to be used for multi-dimensional elliptic flow computations [3]. Since the low turbulence region almost always exists in elliptic flows in the form of potential core, it is important to conform smooth transition of flow field variables from the high turbulence region to low turbulence region.

For linear elliptic boundary value problems, the convergence rate is given as [17]:

$$||e||_0 = Ch^{k+1} \quad (8)$$

where $||e||_0$, $||e||_0 = (\int_{\Omega} (a - a_h)^2 dx)^{\frac{1}{2}}$, is the zeroth order error norm; Ω is the computational domain; a is the exact solution; a_h is the finite element solution; C is a constant dependent on problems; h is the mesh size; and k is the order of interpolating polynomial. Equation (6) denotes that the convergence rate of the zeroth order error norm would be 3 if quadratic elements are used. For parabolic differential equations, the error norm is bounded by the discretization error in time domain and

that of the spatial domain [18]. For the boundary layer flows, the previous computational experiment showed that the convergence rate is approximately 2.6 for fixed step-size (Δx) in flow direction [6]. This degeneration of convergence rate was caused by the discretization error in the flow-direction (time-like domain) as well as the feed-back effect of the non-linear time-like derivative, $u(\partial u / \partial x)$. Nevertheless, considering that the error norm is defined in global sense, that the convergence rate is still higher than two, and that h is the real mesh size used in computations, it may be claimed that the quadratic finite element computation is more accurate than a second-order-accurate finite differencing scheme for which the convergence rate is obtained from the Taylor series expansion as the mesh size becomes infinitely small. This statement can be supported by many available computational results on heat conduction problems and laminar flow calculations. Based on these facts, it can also be claimed that the numerical diffusion involved in the finite element computation would be less compared to a second-order-accurate finite differencing scheme. This can partly explain why the experimentally observed c_μ -variation in the turbulent flow field needs to be incorporated into the finite element computation in order to achieve the realizability (i.e., the turbulent kinetic energy and the dissipation rate need to be positive) of turbulence quantities.

COMPUTATIONAL RESULTS

All of the computations were performed on the physical domain using physical dimensions; and the material property data used are the density, ρ , equal to 1.225 kg/m³, and the molecular viscosity, μ , equal to 0.17854×10^{-4} kg/m-sec. For all of the example cases, 45 unequally spaced quadratic elements were used to discretize the transverse domain, unless otherwise specified. The convergence criterion used is given as:

$$\left| \frac{a_j^{n+1} - a_j^n}{a_j^{n+1}} \right| < 1 \times 10^{-7}, \quad j = 1, N \quad (9)$$

where the superscript n denotes iteration level, the subscript j denotes each degree of freedom, and N denotes the total degree of freedom.

1. Fully Developed Channel Flow

Experimental data for the fully developed channel flow used herein can be found in Laufer [19]. Half of the channel width is equal to 0.0625 m, the center line mean velocity is equal to 7.07 m/sec, the Reynolds number based on these two parameters is approximately 30,800, the pressure gradient is equal to $-1.405 \text{ kg-m/sec}^2\text{-m}^3$, and the wall friction velocity, u_τ is equal to 0.270 m/sec.

The computational domain which extends from $y = 0.005$ m near the wall, which corresponds to $y^+ = 100$, to $y = 0.0635$ m at the center of the channel was discretized using 20 equally spaced quadratic elements. Near $y^+ = 40$ and below, high Reynolds number turbulence models may not yield good predictions unless these are modified by including low turbulence Reynolds number effects.

The Dirichlet boundary conditions for u and k at the near wall region were obtained from experimental data, whereas the boundary condition for ϵ was obtained from the mixing length assumption given below.

$$\ell = c_{\mu f}^{\frac{1}{4}} \ell_m$$

$$\ell_m = \kappa y \quad (10)$$

$$\epsilon = c_{\mu f} k^{3/2} / \ell$$

where ℓ is the turbulence length scale, ℓ_m is the mixing length, $\kappa = 0.41$, and $c_{\mu f} = 0.09$. The near wall boundary conditions used are: $u = 5.084$ m/sec; $k = 0.213$ m²/sec²; and $\epsilon = 10.64$ m²/sec³.

A total of 84 iterations were used to achieve the convergence criterion given previously. The computational results for the velocity, the turbulent kinetic energy and the Reynolds stress are compared with experimental data in Figure 2.

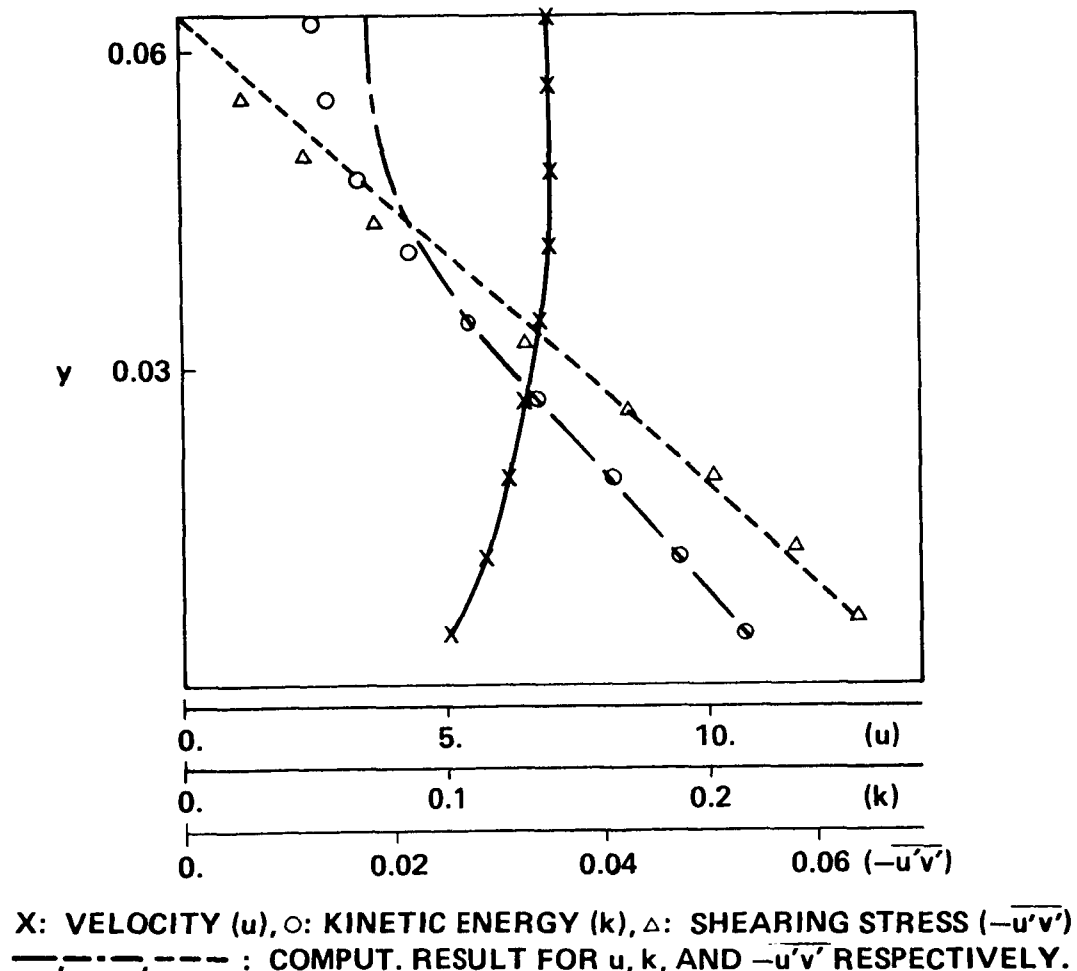
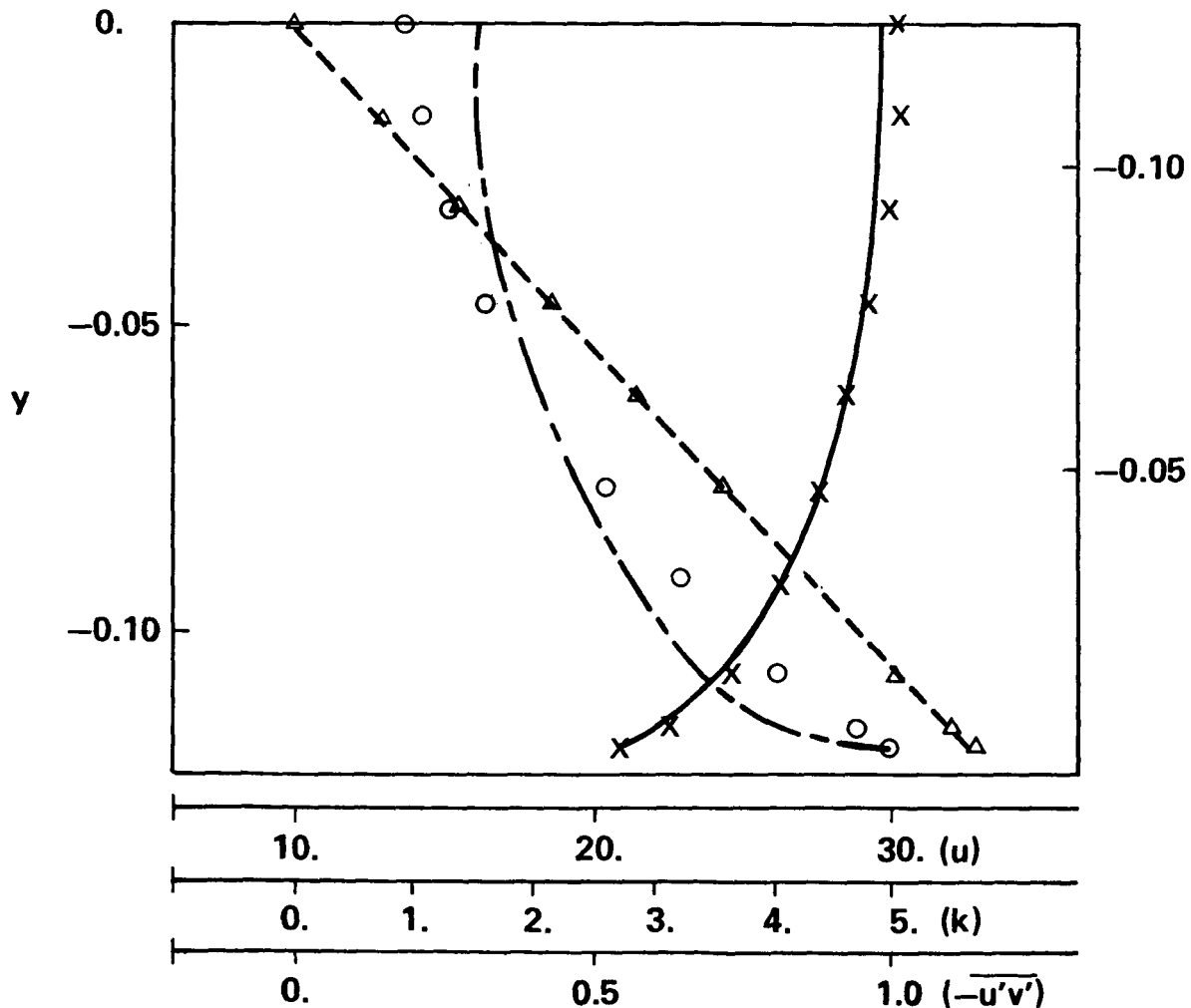


Figure 2. Fully developed channel flow.

2. Fully Developed Pipe Flow

The fully developed pipe flow is another case of elliptic boundary layer flow. The experimental data used can be found in Laufer [20]. The diameter of the pipe is 0.24688 m, the center line velocity is 30.48 m/sec, the Reynolds number based on these two parameters is 500,000, the pressure gradient in the flow direction is equal to $-23.05 \text{ kg-m/sec}^2\text{-m}^3$, and the wall friction velocity is equal to 1.078 m/sec.

The computational domain extending from $y = 0 \text{ m}$ at the center of the pipe to $y = 0.1192 \text{ m}$ at the near wall region, which corresponds to $y^+ = 300$, were discretized using 20 equally spaced quadratic elements. The near wall boundary conditions obtained from experimental data are given as: $u = 20 \text{ m/sec}$, $k = 4.93 \text{ m}^2/\text{sec}^2$, and $\epsilon = 1000 \text{ m}^2/\text{sec}^3$. It took 100 iterations to achieve the same prescribed convergence criterion. The computational results are compared with experimental data in Figure 3.



NOTATIONS ARE THE SAME AS IN FIGURE 1.

Figure 3. Fully developed pipe flow.

3. Flat Plate Boundary Layer Flow Under Vanishing Pressure Gradient

The Wiehardts and Tillman flat plate boundary layer flow [21] is considered below. Another case of equilibrium boundary layer flow with zero pressure gradient can be found in Klebanoff [16]. Both of the flat plate boundary layer flows are self-similar flows. Experimental wall shearing stresses are presented in Wiehardts and Tillmann [21], whereas self-similar Reynolds stresses are given in Klebanoff [16]. In the following computation, the initial condition data for velocity were obtained from Wiehardts and Tillmann [21]; and the turbulent kinetic energy from Klebanoff [16].

The free stream velocity is equal to 33 m/sec and the free stream turbulence level is 0.25 percent. The transverse computational domain extending from $y = 0.001$ m at the near wall region, which corresponds to $y^+ = 100$, to $y = 0.112$ m at the free stream region was discretized using 45 unequally spaced quadratic elements. The computational domain in the flow direction, which extends from $x = 0.937$ m up to $x = 4.987$ m was discretized using 600 line-steps.

Development of the wall shearing stress along the flow direction is shown in Figure 4; the computed velocity profile, the kinetic energy profile, and the Reynolds stress are compared with experimental data in Figure 5. Approximately 14 iterations were required for each line-step.

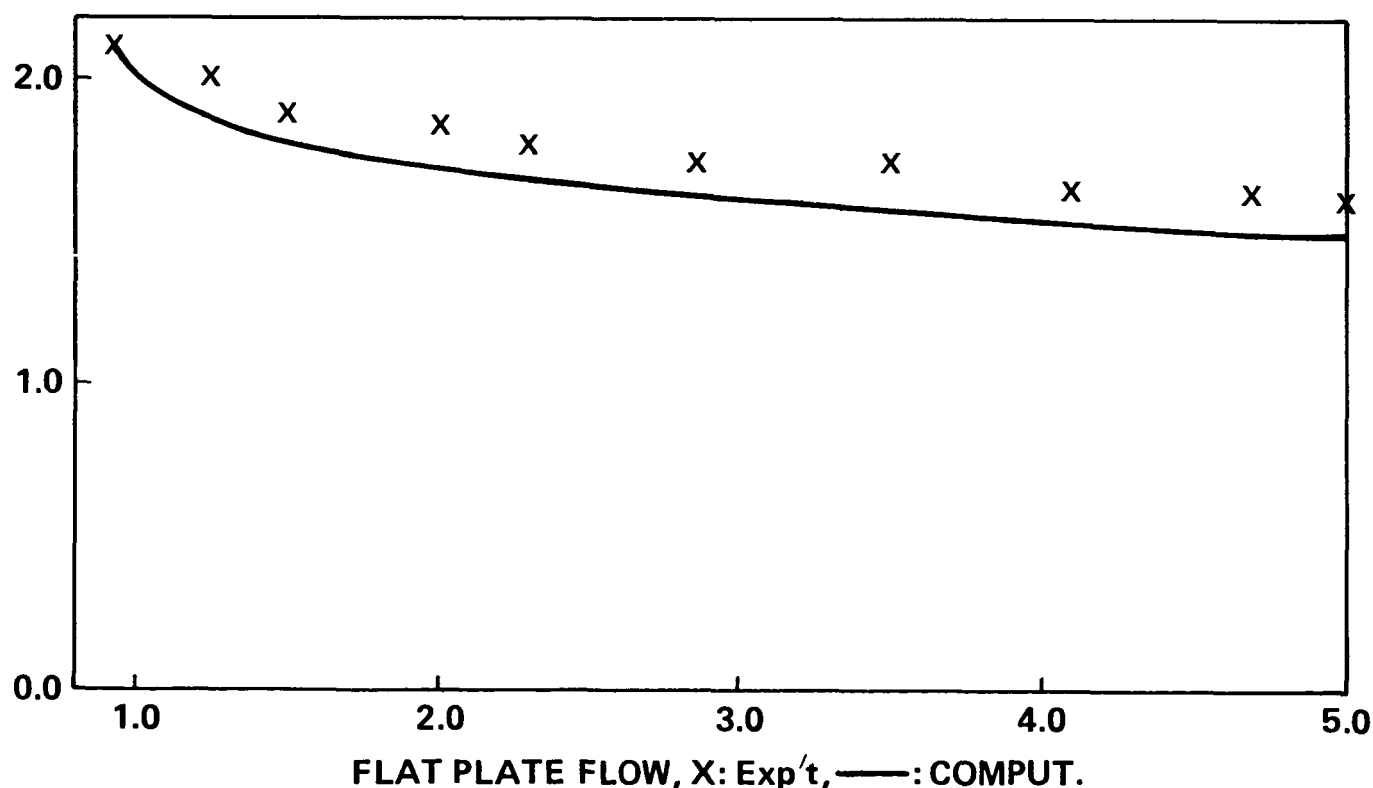


Figure 4. Wall shearing stress for the flat plate flow.

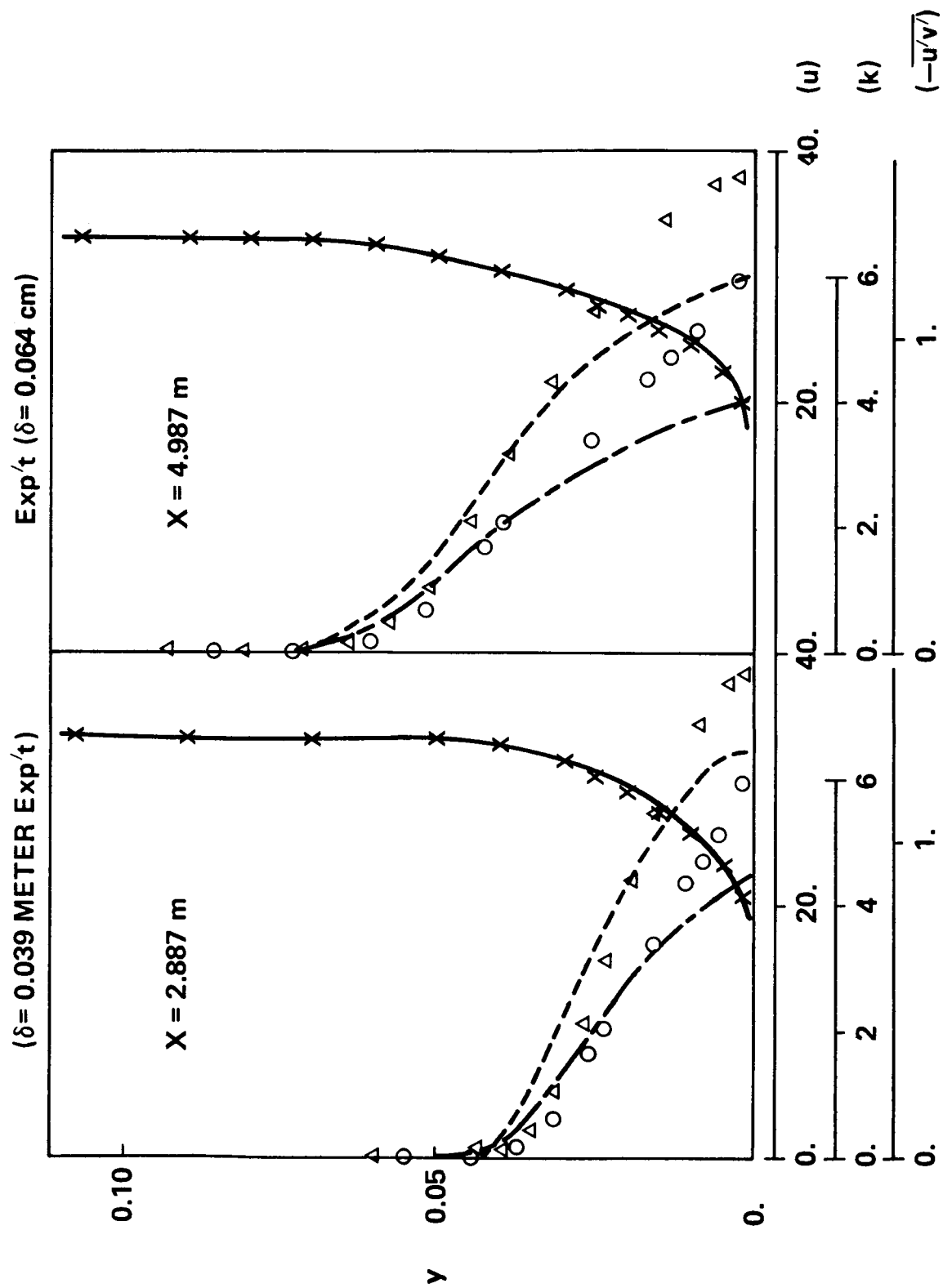


Figure 5. Flat plate flow with zero pressure gradient.

4. A Plane Jet Exhausting into a Moving Stream

A plane jet exhausting into a moving stream is considered below, the experimental data of which can be found in Bradbury [22].

The transverse domain extends from center line of the jet, $y = 0$, to $y = 0.1$ m which is approximately 12.5 times of the half jet width (the half jet width is defined as a distance from the center line of jet to a location where the excess velocity is half of the center line excess velocity). The computational domain in flow direction starting from $x = 0.095$ m ($x/d = 10$, $d = 0.009525$ m is the jet exit width) to $x = 0.65$ m ($x/d = 70$) was discretized by 580 line-steps.

Decay of the center line velocity and evolution of the half jet width along the flow direction compares favorably with experimental data as shown in Figure 6. The computed velocity profile, turbulent kinetic energy profile, and the Reynolds stress are compared with experimental data in Figure 7 at two flow direction locations. These profiles compare favorably with experimental data at the middle of the flow direction domain, whereas these profiles compare less favorably with experimental data at the end of the computational domain. These degenerated solutions may be due to less appropriate c_μ function. But the global features such as the growth of the half jet width were found to be less sensitive to the c_μ function.

An average of 11 iterations were required to satisfy the convergence criterion for each line-step.

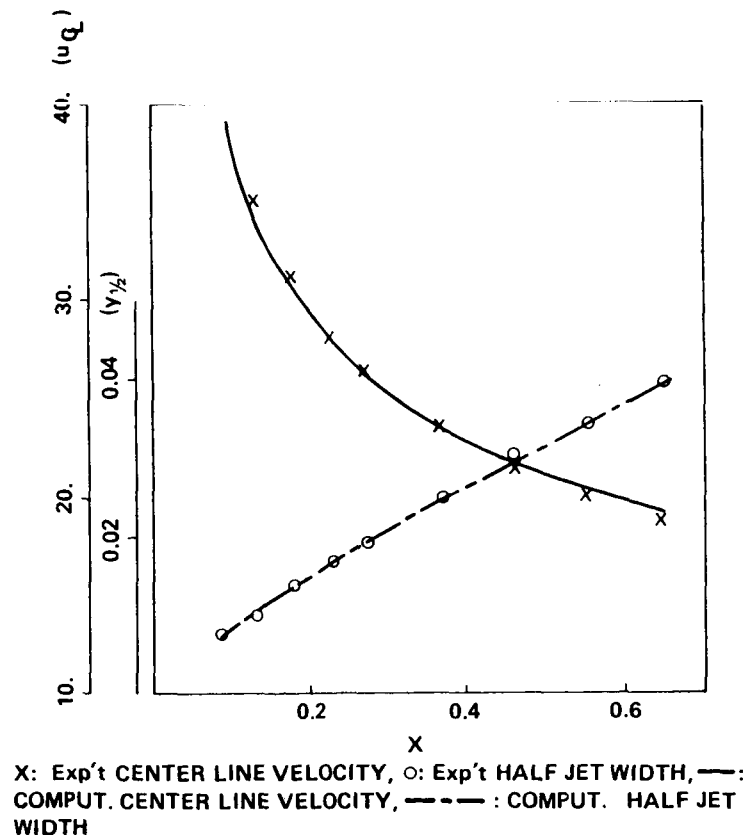
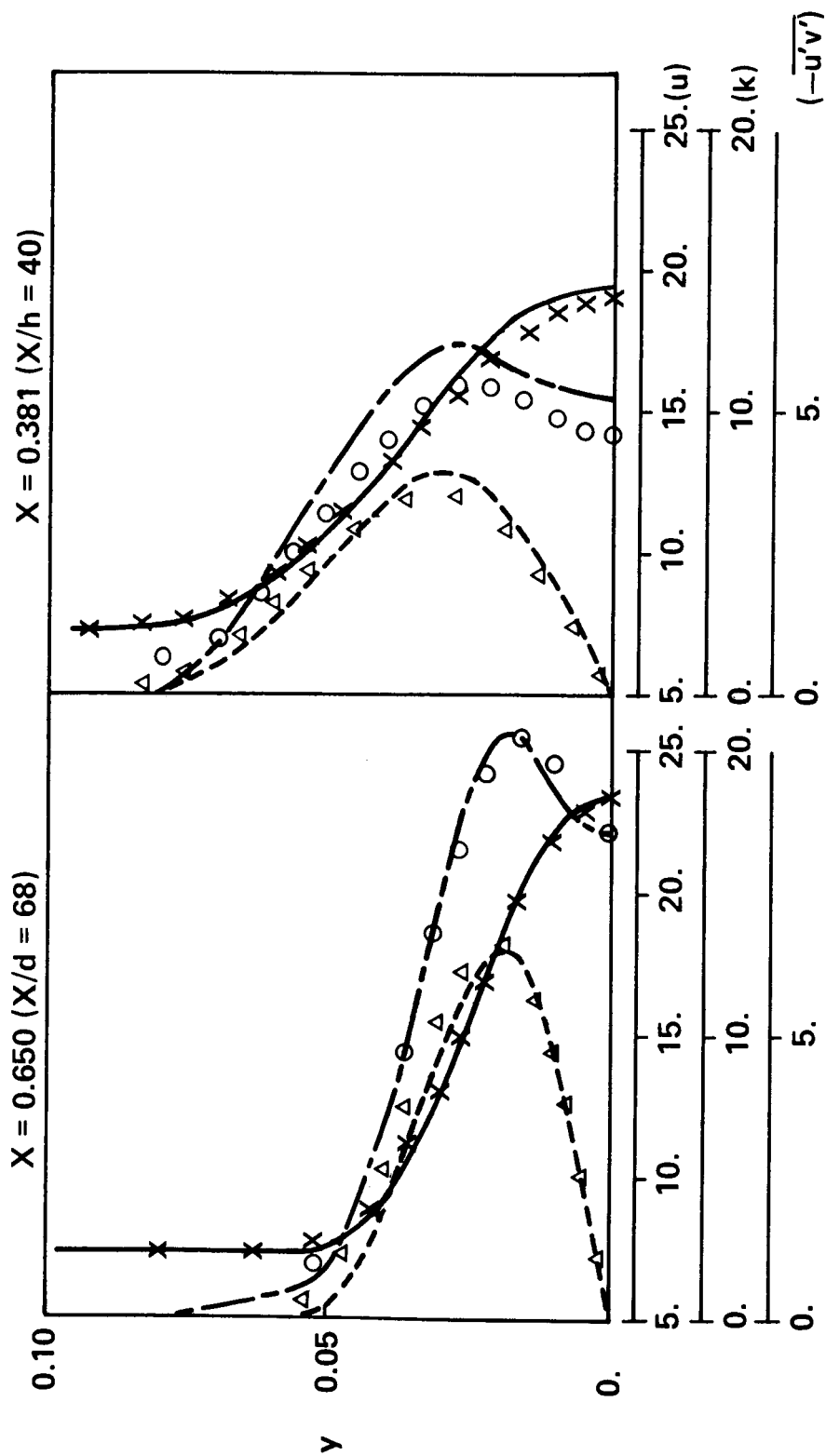


Figure 6. A plane jet exhausting into a moving stream.



X: Exp't VELOCITY, O: Exp't TURBULENT KINETIC ENERGY, Δ : Exp't $-u'v'$; ---, - - - - , AND dash-dot: COMPUT. VELOCITY, TURBULENT KINETIC ENERGY, AND $-u'v'$ RESPECTIVELY

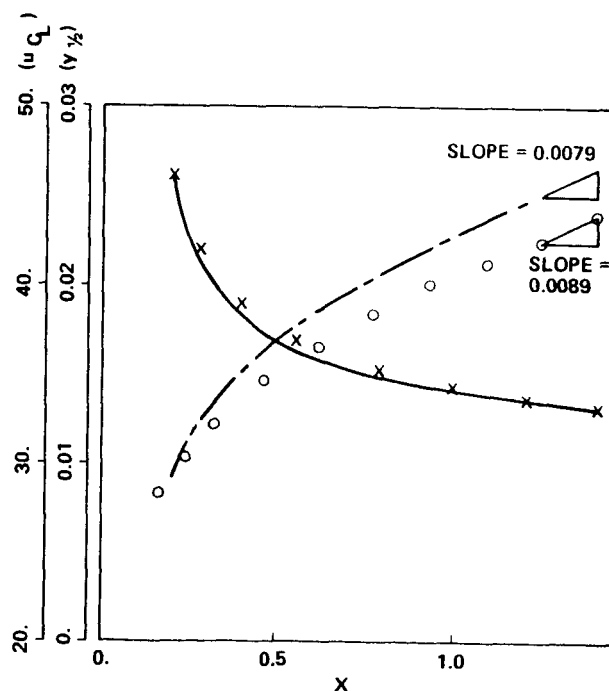
Figure 7. A plane jet exhausting into a moving stream.

5. A Circular Jet Exhausting Into a Moving Stream

Anomaly between plane jet and circular jet has been discussed more than enough number of times from the early days of $k-\epsilon$ type turbulence model development. Recently, the anomaly has been somewhat resolved in Hanjelic and Launder [12] by introducing irrotational strain into the turbulence equations. Unfortunately, the improvement cannot be carried over to computation of multi-dimensional elliptic flows. The advantage of the present turbulence model also lies in the fact that the improvement can be carried over to elliptic flow computations, as can be found in Reference 7.

A circular jet experiment due to Antonia and Bilger [23] is considered herein. The turbulent kinetic energy profile for initial condition data was prepared from the experimental data of $\sqrt{(u')^2}/u_0$, where u' is the fluctuating velocity in the flow direction and u_0 is the center-line excess velocity, by assuming that the turbulent kinetic energy would be approximately 1.2 times the flow direction normal Reynolds stress. The computational domain in the transverse direction extends from $y = 0$ m, the center-line, to $y = 0.084$ m, which corresponds to approximately nine times the half jet width. The flow direction domain starting from $x = 0.2$ m ($x/d = 40$, where $d = 0.00528$ m is the diameter of the jet) to $x = 1.4$ m ($x/d = 265$) was discretized into 1200 line-steps. An average of six iterations were required for each line-step to achieve the convergence criterion.

Computational results showed that the flow field re-developed due to the inaccurate turbulent kinetic energy data; and that a similarity state which is slightly different from experimental data was achieved in the far down-stream region. Decay of the center-line velocity and the growth of the half jet width are shown in Figure 8, where it can be seen that the spreading rate at the far down-stream is close to that of the experimental data.



NOTATIONS ARE THE SAME AS IN FIGURE 2.

Figure 8. A circular jet exhausting into a moving stream.

Due to the re-development of the flow field, the computational results are compared with experimental data in similarity coordinate (Fig. 9). It can be seen in Figure 9 that the velocity profile is flatter than that of the experimental data in the center region of the jet, and that the gradient of velocity profile is stiffer than experimental data in the middle region of the jet. The Reynolds stress profile obtained by using the Boussinesq eddy viscosity assumption that $\overline{u'v'} = \nu_t \partial u / \partial y$ is higher than experimental data due to the stiffer velocity gradient in the same middle region. These discrepancies are due to the deficiency of the c_μ function, and these degenerated computational results were not obtained in the finite difference computation of the same flow case using a constant c_μ [7].

6. A Wall Jet Issuing into a Moving Stream

The wall jet is a boundary layer flow which finds a great number of applications in engineering processes. It is used in many different situations of film cooling processes and in preventing separation of boundary layer flows. The wall jet provides a serious test case for a numerical method as well as a turbulence model, since both of these must be able to predict the behavior of wall bounded boundary layer flows and jets separately. Finite difference computation of wall jet flows can be found in Ljuboja and Rodi [24] among many others.

One of the most complete experimental data for the wall jet flows can be found in Irwin [25]. A configuration of wall jet is shown in Figure 10, where b is the jet slot height, U_j is the jet exit velocity, $u_e(x)$ is the free stream velocity, u_0 is the maximum excess velocity, u_m ($u_m = u_0 + u_e$) is the maximum velocity, y_m is a distance from the wall to a location where $u = u_m$, and $y_{1/2}$ is the half jet width defined as the distance from the wall to the outer side location where $u = u_0/2 + u_e$. Input data used in computation of the flow were obtained directly and/or by curve-fitting the experimental data [25]. These are: $b = 0.00673$ m, $U_j = 60.64$ m/sec; and the external free stream velocity and the length-scale of the flow field are given below:

$$u_e(x) = \frac{1}{1.65} \bar{U}_j [0.12052 (x/b) + 0.98425]^{-0.448} \quad (11)$$

$$\frac{y_0(x)}{b} = 0.04394 (x/b) + 0.3819 \quad (12)$$

The computational domain extends from $y = 0.002$ m to $y = 0.08$ m in the transverse direction; and from $x = 0.5532$ m ($x/b = 82.2$) to $x = 1.6892$ m ($x/b = 251$) in the flow direction. The flow direction domain was discretized by 1135 line-steps, and an average of 14 iterations were required for each line-step to achieve the same convergence criterion given previously. It can be seen in Figures 11 and 12 that computational results compare favorably with experimental data in every detail.

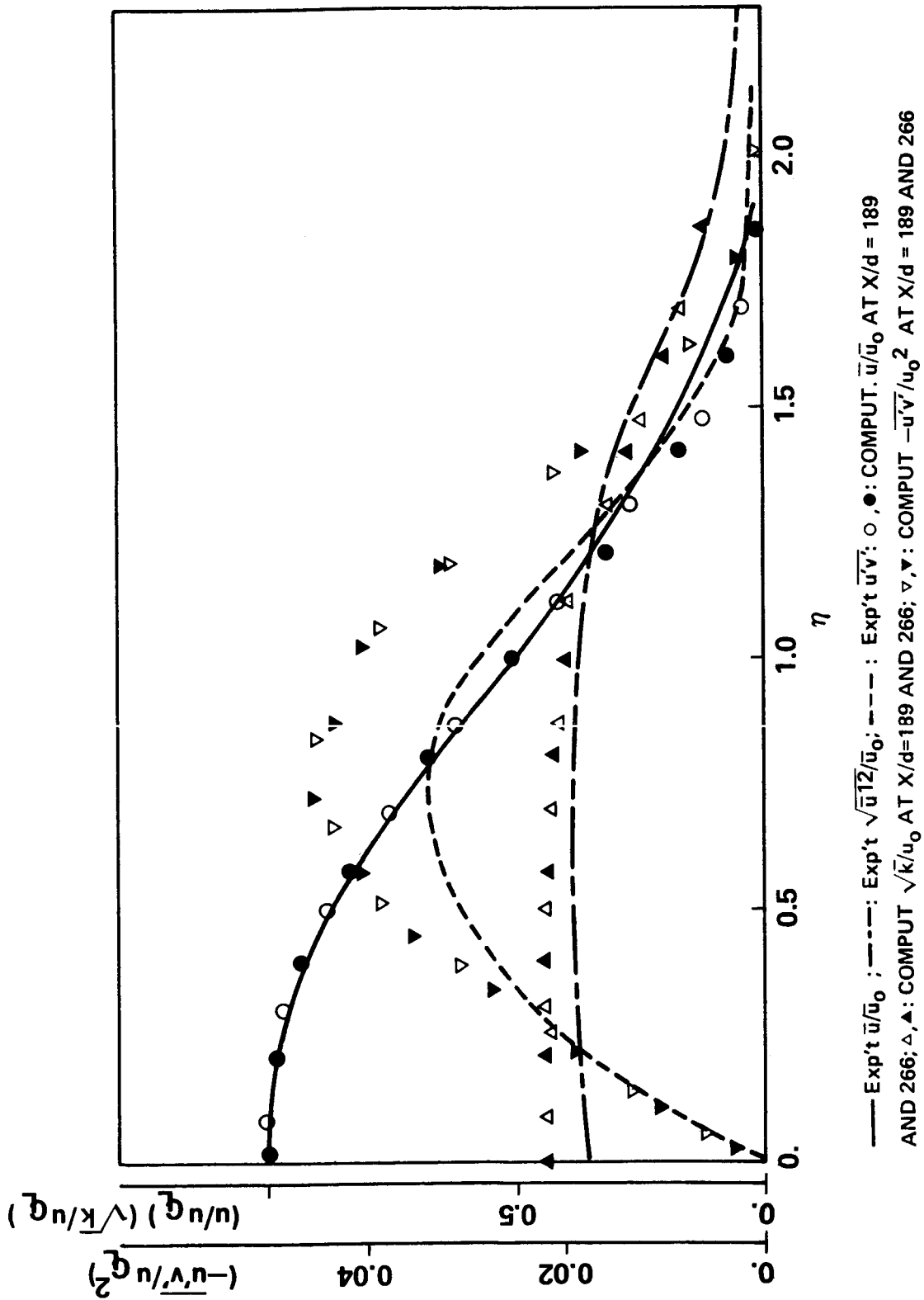


Figure 9. A circular jet exhausting into a moving stream.

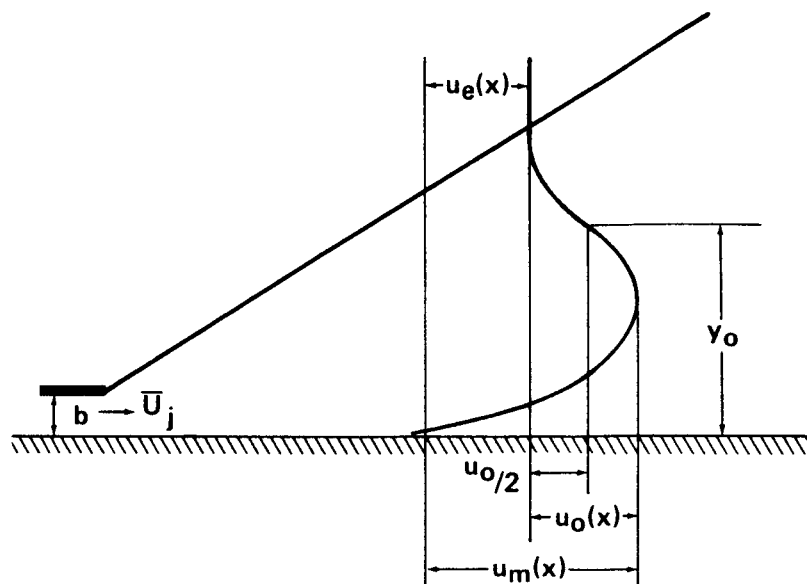


Figure 10. Configuration of a wall-jet flow.

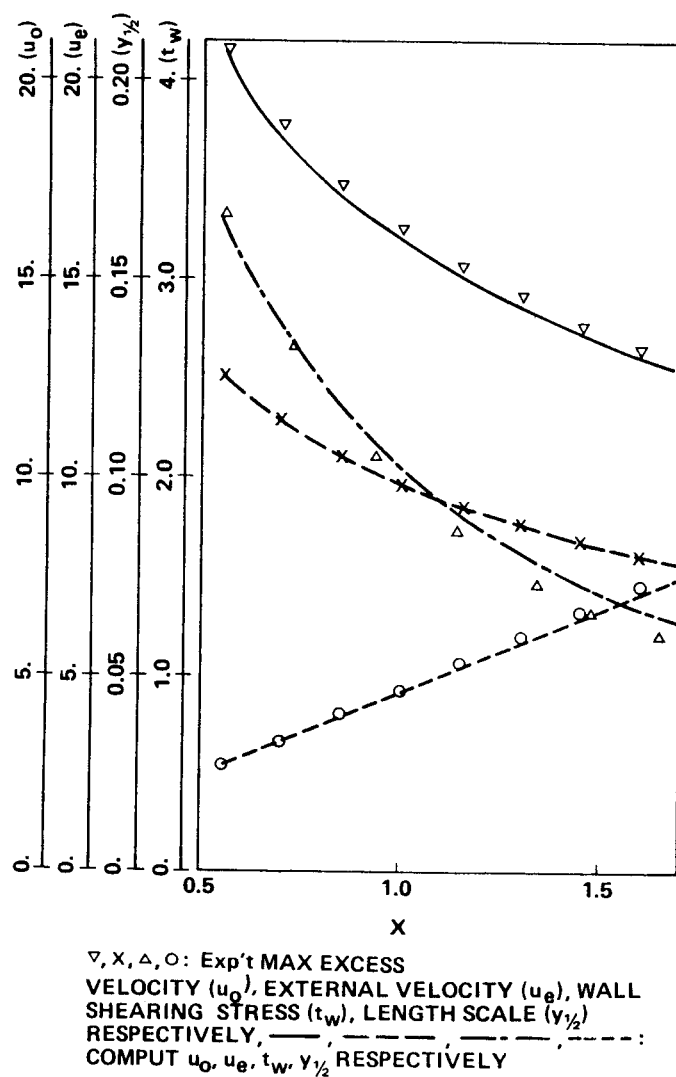
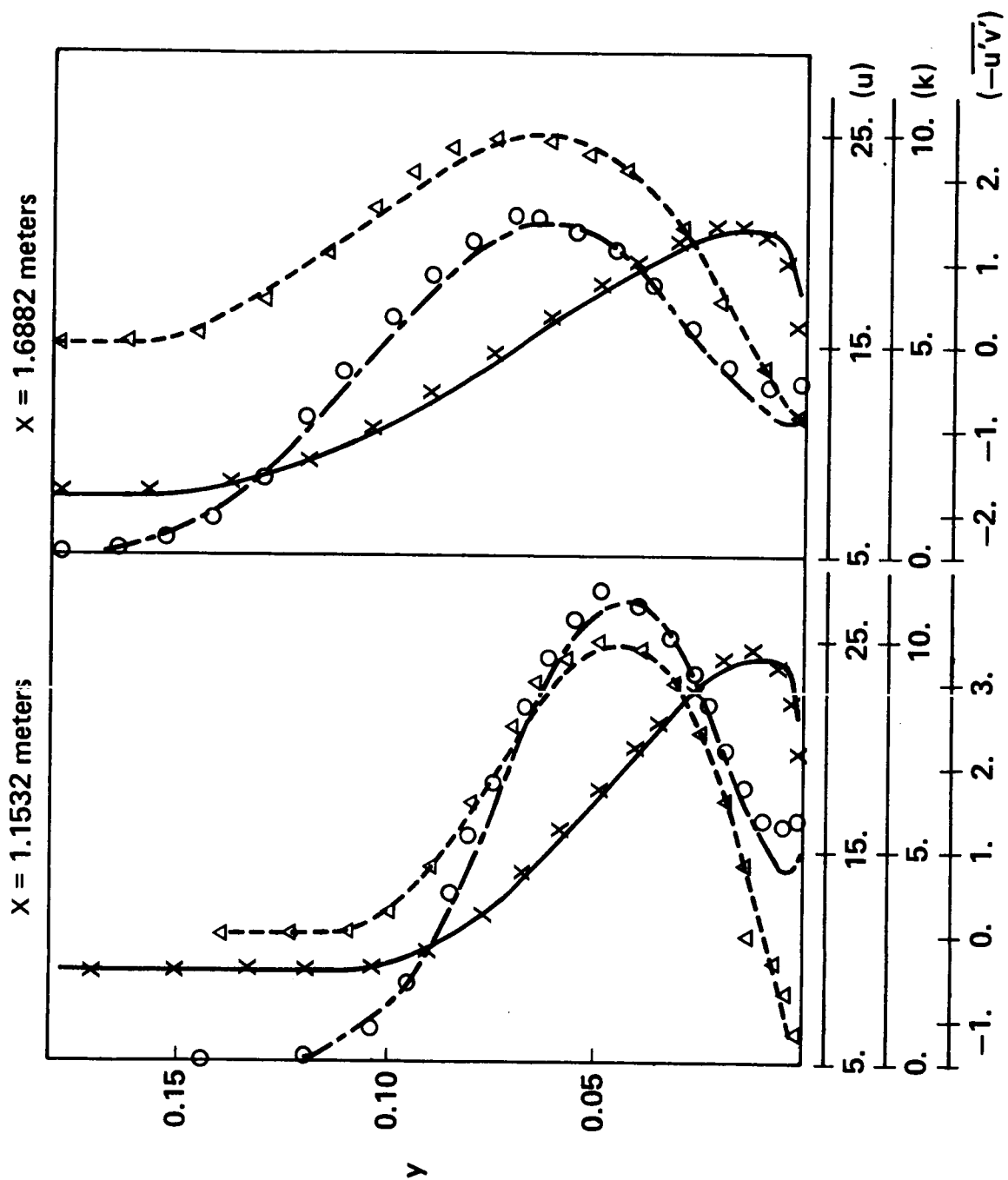


Figure 11. Wall-jet flow.



NOTATIONS ARE THE SAME AS IN FIGURE 3.

Figure 12. A wall-jet flow.

CONCLUSIONS

An algebraic stress turbulence model was presented together with finite element computation of a few turbulent flows. Experimentally deduced c_μ curves reveal that the value of c_μ needs to be close to that of the equilibrium condition (i.e., the production rate is the same as the dissipation rate) at the center region of jets where production rate is small but the turbulent kinetic energy is high. The center region of jets is apparently a high turbulence region even though the production rate is small. It is believed that further improvement of the c_μ function to incorporate the experimentally observed behavior of c_μ at the center region of jets will undoubtedly improve the turbulence model proposed. This fact can be further supported by the finite difference computation of the same turbulent boundary layer flows using the same turbulence model but with a constant c_μ [7], where significantly improved computational results over the standard $k-\epsilon$ turbulence model can be found not only for turbulent boundary layer flows but also for separated and swirling elliptic flows. In the present finite element computation, use of the c_μ function was indispensable to achieve realizability (i.e., the turbulent kinetic energy and the dissipation rate cannot become negative). In fact, most of the $k-\epsilon$ type turbulence models were able to run in the present boundary layer flow code [3] without any numerical difficulty if the c_μ function was included into those turbulence models. In this sense, the present study clarified one of the fundamental differences between the finite element method and the finite difference method.

REFERENCES

1. Coles, D. E. and Hirst, E. A., editors: Proc. Computation of Turbulent Boundary Layers, AFOSR-IFP-Stanford Conference, 1968.
2. Kline, S. J., Cantwell, B. J., and Lilley, G. M., editors: Proc. Complex Turbulent Flows, AFOSR-HTTM-Stanford Conference, 1980-1981.
3. Kim, S.-W., and Chen, Y.-S.: A Finite Element Computational Procedure for Turbulent Boundary Layer Flows. In preparation.
4. Taylor, C., Thomas, C. E., and Morgan, K.: F.E.M. and the Two Equation Model of Turbulence. Editors C. Taylor and K. Morgan, Computational Techniques in Transient and Turbulent Flows, Vol. 2, 1981.
5. FIDAP, A Fluid Dynamics Analysis Package, Boeing Aircraft Company, 1984.
6. Kim, S.-W., and Payne, F. R.: Finite Element Analysis of Incompressible Laminar Boundary Layer Flows. Int. J. Num. Meth. Fluids, Vol. 5, pp. 545-560, 1985.
7. Chen, Y.-S., and Kim, S.-W.: Computation of Turbulent Flows with an Extended $k-\epsilon$ turbulence closure model. NASA-CR, in preparation.
8. Hanjalic, K., and Launder, B. E.: Contribution Towards a Reynolds-Stress Closure for Low-Reynolds-Number Turbulence. J. Fluid Mech., Vol. 74, pp. 593-610, 1976.
9. Rodi, W.: The Prediction of Free Boundary Layers by Use of a Two-Equation Model of Turbulence. Ph.D. Thesis, University of London, London, 1972.
10. Launder, B. E.: A Generalized Algebraic Stress Transport Hypothesis. J. AIAA, Vol. 20, pp. 436-437, 1982.
11. Pope, S. B.: An Explanation of the Turbulent Round-Jet/Plane-Jet Anomaly. J. AIAA, Vol. 16, pp. 279-281, 1978.
12. Hanjalic, K., and Launder, B. E.: Sensitizing the Dissipation Equation to Irrotational Strains. Transactions of ASME, Vol. 102, pp. 34-40, 1980.
13. Hanjalic, K., Launder, B. E., and Schiestel, R.: Multiple-Time-Scale Concepts in Turbulent Shear Flows. Editors L. J. S. Bradbury et al., Turbulent Shear Flows, Vol. 2, pp. 36-49, Springer-Verlag, New York, 1980.
14. Harris, V. G., Graham, J. A. H., and Corrsin, S.: Further Experiments in Nearly Homogeneous Turbulent Shear Flow. J. Fluid Mechanics, Vol. 81, pp. 657- 687, 1977.
15. Harlow, F. H., and Nakayama, P. I.: Transport of Turbulence Energy Decay Rate. Los Alamos Sci. Lab., LA3854, 1968.
16. Klebanoff, P. S.: Characteristics of Turbulence in a Boundary Layer with Zero Pressure Gradient. NACA CR-1247, 1954.

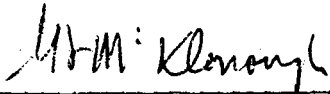
17. Becker, E. B., Carey, G. F., and Oden, J. T.: Finite Elements - An Introduction. Prentice-Hall, J. J., 1981.
18. Oden, J. T., and Reddy, J. N.: An Introduction to the Mathematical Theory of Finite Elements. Wiley-Interscience, New York, 1976.
19. Laufer, J.: Investigation of Turbulent Flow in a Two-Dimensional Channel. NACA CR-1053, 1949.
20. Laufer, J.: The Structure of Turbulence in Fully Developed Pipe Flow. NACA TR-1174, 1954.
21. Wiehard, K., and Tillmann, W.: Wiehard Flat Plate Flow, Flow 1400. Editors D. E. Coles and E. A. Hirst, Proc. Computation of Turbulent Boundary Layers, AFOSR-IFP-Stanford Conference, 1968.
22. Bradbury, L. J. S.: The Structure of a Self-Preserving Turbulent Plane Jet. J. Fluid Mech., Vol. 23, 1965, pp. 31-64.
23. Antonia, R. A., and Bilger, R. W.: An Experimental Investigation of an Axisymmetric Jet in a Co-Flowing Air Stream. J. Fluid Mechanics, Vol. 61, pp. 805-922, 1973.
24. Ljuobja, M., and Rodi, W.: Calculation of Turbulent Wall Jets with an Algebraic Stress Model. Transactions of the ASME, Vol. 102, pp. 350-356, 1980.
25. Irwin, H. P. A. H.: Measurements in a Self-Preserving Plane Wall Jet in a Positive Pressure Gradient. J. Fluid Mech., Vol. 61, pp. 33-63, 1973.

APPROVAL

COMPUTATION OF TURBULENT BOUNDARY LAYER FLOWS WITH AN ALGEBRAIC STRESS TURBULENCE MODEL

By Sang-Wook Kim and Yen-Sen Chen

The information in this report has been reviewed for technical content. Review of any information concerning Department of Defense or nuclear energy activities or programs has been made by the MSFC Security Classification Officer. This report, in its entirety, has been determined to be unclassified.



G. F. McDONOUGH

Director, Systems Dynamics Laboratory